μ-Mesonic X-Ray Energies and Nuclear Radii for Fourteen Elements from $Z=12$ to 50*

H. L. ANDERSON AND C. S. JOHNSON
The Enrico Fermi Institute for Nuclear Studies, The University of Chicago, Chicago, Illinois

AND

E. P. HINCKS
Division of Pure Physics, National Research Council of Canada, Ottawa, Ontario, Canada

(Received 6 February 1963)

Precise measurements of μ-mesonic x rays have been made using a NaI scintillation crystal spectrometer. The $2p-1s$ transition energies were determined for fourteen elements ranging from $Z=12$ (Mg) to $Z=50$ (Sn). The $3d-2p$ transition energies were also measured for seven of these elements. The results have been interpreted to give a measure of the radial extent of the nuclear charge based on a Dirac theory of the μ-mesonic atom, correcting for the vacuum polarization but taking other possible perturbing effects (e.g., nuclear polarization) to be small. The $2p-1s$ transition energy depends essentially on the second moment of the charge distribution, somewhat independently of the detail of the shape. It is convenient, therefore, to use the equivalent radius $R_{eq}=(5\langle r^2\rangle/3)^{1/2}$ which refers to a sphere of uniform charge distribution having a mean square radius $\langle r^2\rangle$. Our values of $r_0=R_{eq}/A^{1/3}$ are within $(1.23\pm0.02)\times10^{-13}$ cm for all nine of our elements between $A=35$ (Cl) and $A=119$ (Sn). There is general, but not detailed agreement with the radii that have been deduced from the Stanford electron scattering experiments.

I. INTRODUCTION

A FEW months ago[1] we reported the measurement of several μ-mesonic $2p-1s$ transition energies which were somewhat higher than what was expected according to careful theoretical calculations by Ford and Wills.[2] In order to verify the discrepancy in greater detail, we repeated the experiment with improved technique, remeasuring some of the elements and extending the measurements to include others. The new measurements confirmed the earlier result making more serious the question of the discrepancy.

As is well known, the $2p-1s$ transition energies for a point nucleus are given approximately by the simple Bohr formula,

$$E(2p-1s)=\tfrac{3}{4}(13.6)Z^2\bar{\mu}\ \text{eV}, \qquad (1)$$

where Z is the nuclear charge and $\bar{\mu}$ is the reduced muon mass in units of the electron mass. Thus, E/Z^2 is a constant except for the small reduced mass effect. In Fig. 1 we have plotted E/Z^2 as a function of Z, (a) according to Eq. (1) above, (b) according to the solution of the Dirac equation for a point nucleus taking relativity and spin-orbit interaction into account,[3] and (c) according to Ford and Wills' solution of the Dirac equation for a finite nucleus including the effect of vacuum polarization.

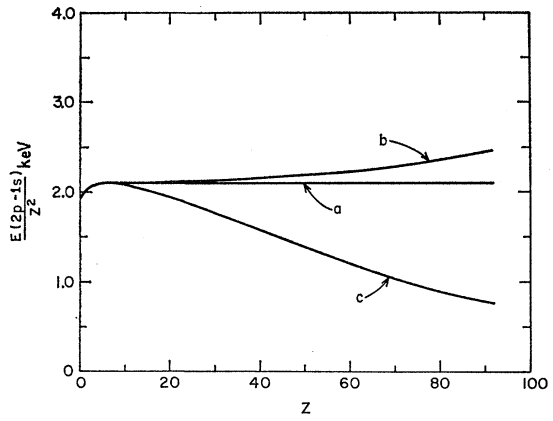

FIG. 1. The $2p-1s$ transition energies divided by Z^2 for μ-mesonic atoms. (a) for a point nucleus in nonrelativistic theory, (b) in relativistic Dirac theory, and (c) taking finite size and vacuum polarization effects into account, according to Ford and Wills (reference 2).

It is evident that the finite nuclear size has an appreciable effect on the transition energy. For example, in the case of Mn ($Z=25$), relativity and spin-orbit interactions increase the transition energy by 1%. Vacuum polarization causes a further increase of almost 1%, but the finite extension of the nuclear charge causes a decrease of 14%. This last and most important effect depends on the particular choice of the nuclear charge distribution. For light nuclei, the shift in the transition energy is determined primarily by $\langle r^2\rangle$, the mean square radius of the charge distribution.[4]

In the Ford and Wills calculation, the choice of charge distribution came from an analysis of the Stanford electron scattering experiments and we had little reason to question this until it was pointed out to us by D. G. Ravenhall that a different analysis[5] of the same data using a somewhat different shape function gave a different value for $\langle r^2\rangle$.

* Research supported by the Office of Naval Research.

[1] C. S. Johnson, E. P. Hincks, and H. L. Anderson, Phys. Rev. **125**, 2102 (1962).

[2] K. W. Ford and J. G. Wills, Los Alamos Scientific Laboratory Report LAMS-2387, 1960 (unpublished); Nucl. Phys. **35**, 295 (1962).

[3] The $2p-1s$ energy is measured from the center of gravity of the p-doublet, i.e., $E(p)=\frac{2}{3}E(2p_{3/2})+\frac{1}{3}E(2p_{1/2})$.

[4] L. N. Cooper and E. M. Henley, Phys. Rev. **92**, 801 (1953).

[5] B. Hahn, D. G. Ravenhall, and R. Hofstadter, Phys. Rev. **101**, 1131 (1956).

In fact, the value of $\langle r^2 \rangle$ given by Hahn *et al.*[5] for $_{20}Ca^{40}$ is 11% smaller than that used by Ford and Wills. This would increase the transition energy by 1.6%, accounting for a large part of the discrepancy. Moreover, Crannell *et al.*[6] have shown that the absolute cross-section data is in better agreement with the Stanford shape than that used by Ford and Wills. For other nuclei the Stanford group[7] give systematically lower values of $\langle r^2 \rangle$ than those used by Ford and Wills.

These comparisons throw doubt on the validity of Ford and Wills' choice of the nuclear charge distributions. Better agreement is obtained when the comparison is made with the Stanford shapes, but small discrepancies still remain. The μ-mesonic x-ray energies may be affected by nuclear polarization and possibly other nuclear interaction effects[4] but these have not been calculated with good accuracy thus far.

TABLE I. Target description.

Target	Area (cm²) or diameter (cm)	Thickness (g/cm²)	Form[a]
Mg	12.7×12.7	4.6	Metal plates
Al	10.2×10.2	4.8	Metal plate
Si	10.2×10.2	2.6	Powder
P	11.0×11.0	4.2	Powder
S	14.5×14.5	4.5	Powder
Cl	12.7×12.7	4.7	Kel-F plastic[b]
Cl	10.8×10.8	3.1	LiCl powder
Ca	10.3×10.3	4.8	Metal plates
Fe[c]	13.0	4.8	Metal powder
Ni[c]	13.0	4.8	Metal powder
Zn	10.0×10.0	4.8	Metal plate
As	11.0×11.0	5.3	Powder
Zr[c]	13.0	5.0	ZrO_2 powder
Mo	12.8×12.8	5.0	Metal plates
Sn	11.0	5.2	Metal plate

[a] Powdered targets were enclosed in boxes made of $\frac{1}{16}$-in.—thick lucite.
[b] Polychlortrifluorethylene, $(C_2ClF_3)_n$.
[c] These targets were in the shape of cylinders and the dimension given is the diameter.

More accurate μ-mesonic x-ray and electron scattering experiments together would be useful in indicating with greater certainty whether effects other than the extension of the nuclear charge can alter the value of the $2p-1s$ transition energies. In this paper, we describe our new measurements[8] and give the values of nuclear charge radius to which they correspond, if nuclear interaction effects are excluded.

II. EXPERIMENT

Several improvements in apparatus and technique were made in this experiment. One possible source of systematic error, the effect of target thickness on line shape, was reduced by performing the calibration runs using gamma sources (in the form of microspheres[9]) which are mixed with powdered target material. In this way, by using identical targets, one with and one without the gamma sources, it was possible to approximate closely with calibration sources the effect of target thickness on the μ-mesonic x rays emitted throughout the target material. In order to improve the linearity of the phototube response, the resistance of the voltage divider chain was reduced and the nonlinearity of the spectrometer was studied more extensively using several gamma sources. A study was also made of the effect of counting rate on the response of the spectrometer. A vibrating target, following Rosen,[10] was used which gave a much improved duty factor and a substantial reduction in the background and possible rate dependent effects.

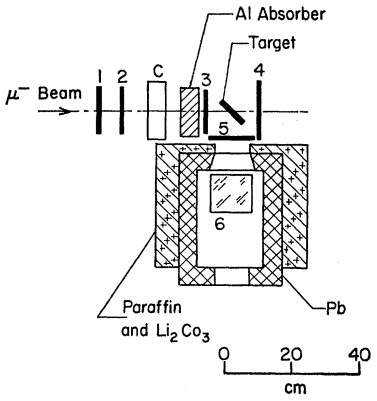

FIG. 2. Side view of the experimental arrangement used for detecting μ-mesonic x rays. Counters 1, 2, 3, 4, and 5 are plastic scintillators. C is a water Čerenkov counter. The NaI detector 6, is situated below the beam level.

The counter arrangement is shown in Fig. 2; it was essentially the same as described in reference 1 with two minor changes. The RCA-6810A used in the Čerenkov counter was replaced by a Phillips 56AVP, and the fringing field of the cyclotron was canceled by degaussing coils surrounding the entire apparatus instead of just counter 6.

The targets were all positioned as shown in Fig. 2 at 45° to the incident beam. A physical description of the various targets used is given in Table I.

III. ELECTRONICS

The electronics was changed from that used in reference 1 and is shown in a block diagram in Fig. 3. The details of the coincidence-anticoincidence circuit are as in reference 1. A stopping muon produces a $(1, 2, 3, \bar{4}+\bar{C})$ event which opens gate No. 1 (1.4×10^{-7} sec full width at half-maximum) through which the anode pulse from counter 6 passes, providing there is

[6] H. Crannell, R. Helm, H. Kendall, J. Oeser, and M. Yearian' Phys. Rev. **121**, 283 (1961).
[7] R. Hofstadter, Ann. Rev. Nucl. Sci. **7**, 231 (1957); and R. Herman and R. Hofstadter, *High Energy Electron Scattering Tables* (Stanford University Press, Stanford, 1960).
[8] A preliminary report has been given to the Washington meeting of the American Physical Society [Bull. Am. Phys. Soc. **7**, 340 (1962)].
[9] Microspheres are tiny ceramic spheres within which the radioactive material is imbedded. They are available from the Minnesota Mining and Manufacturing Company, St. Paul, Minnesota.
[10] J. Rosen, Bull. Am. Phys. Soc. **6**, 9 (1961). See also R. A. Lundy, Phys. Rev. **125**, 1686 (1962).

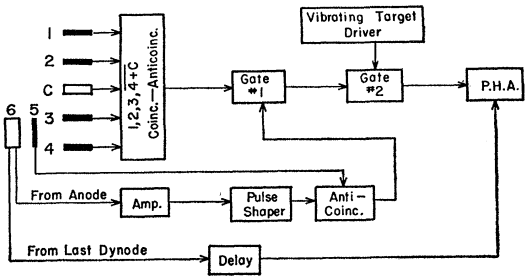

FIG. 3. Block diagram of the electronics. P.H.A. is a 400-channel pulse-height analyzer.

no anticoincidence pulse in counter 5. The anode pulses from counter 6 were limited by transistor amplifiers and clipped to about 2×10^{-8} sec before entering the anticoincidence circuit. The pulses from counter 5 were not clipped and were about 10^{-7} sec wide, full width at half-maximum. Pulses leaving gate No. 1 had to pass through gate No. 2 before they could trigger the 400-channel pulse-height analyzer (Radiation Instrument Development Laboratory Model 34-12), thus allowing it to analyze the dynode pulses from counter 6. Gate No. 2, which was about 3×10^{-3} sec wide, was open only during the beam spill time.

IV. MEASUREMENTS

One or more runs of 60-min duration were made on each target and calibration source spectra were taken at the beginning and end of each run. For the lower Z targets, 1 μC of Na^{22} uniformly distributed throughout a powdered Fe target was used for calibration. For high Z targets, a source of 2.614-MeV gamma rays (ThO_2, also uniformly distributed throughout a powdered Fe target) was used in addition to Na^{22}. Calibration runs were made with the beam off and gates No. 1 and No. 2 disabled so that the pulse-height analyzer was gated by any gamma ray in counter 6 of energy 60 keV or more. The calibration runs were 5 min long, during which time about 6×10^4 counts were recorded in the photopeak of the 1.2736-MeV gamma ray from Na^{22}.

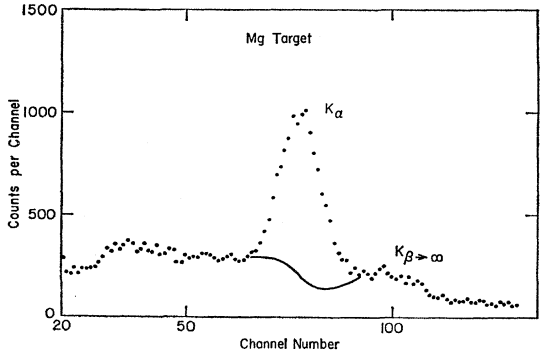

FIG. 4. Pulse-height spectrum of Mg K x rays.

Typical K x-ray spectra obtained from those targets which were not already studied in reference 1 are given in Figs. 4 through 12. Figures 13 through 19 show the

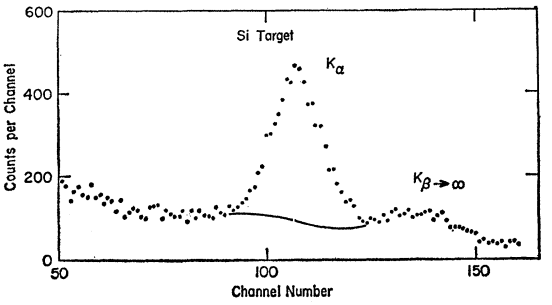

FIG. 5. Pulse-height spectrum of Si K x rays.

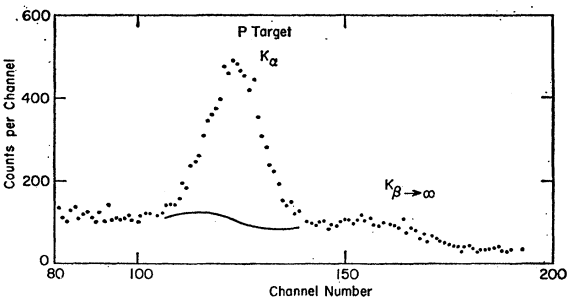

FIG. 6. Pulse-height spectrum of P K x rays.

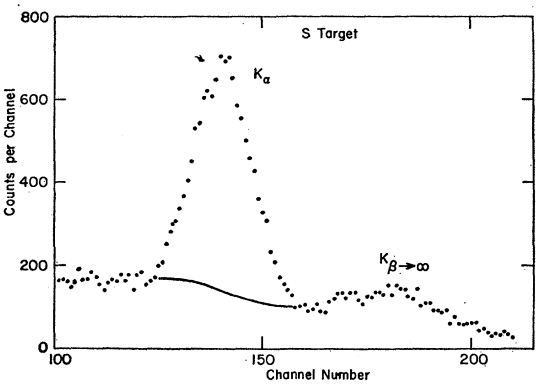

FIG. 7. Pulse-height spectrum of S K x rays.

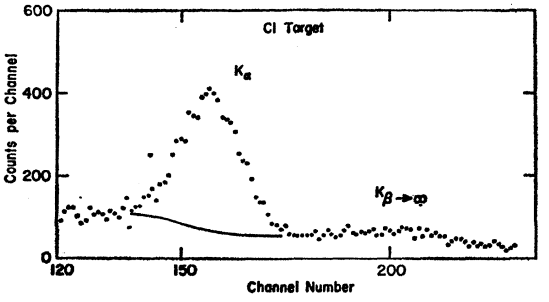

FIG. 8. Pulse-height spectrum of Cl K x rays.

L x-ray spectra. The total subtractions made in evaluating the photopeak positions are indicated in the figures by solid lines.

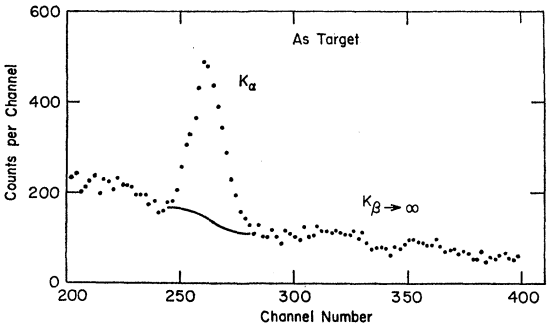

FIG. 9. Pulse-height spectrum of As K x rays.

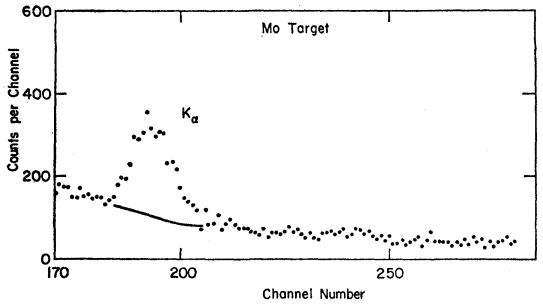

FIG. 10. Pulse-height spectrum of Mo K x rays.

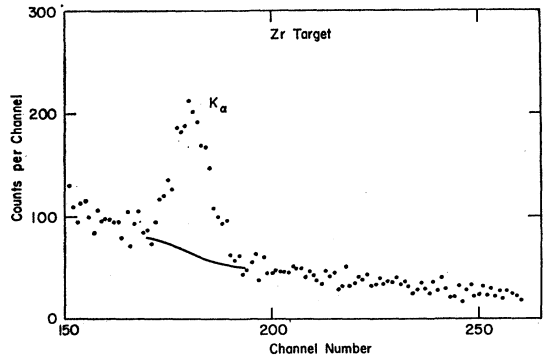

FIG. 11. Pulse-height spectrum of Zr K x rays.

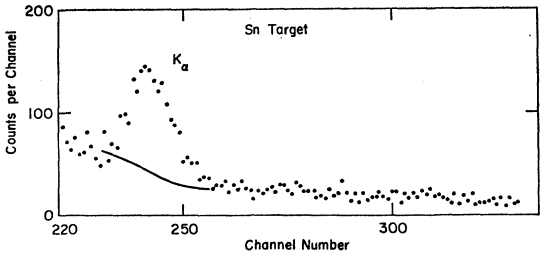

FIG. 12. Pulse-height spectrum of Sn K x rays.

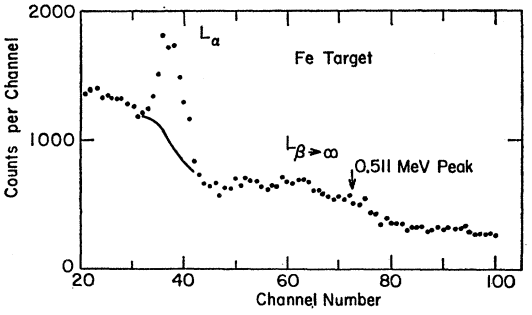

FIG. 13. Pulse-height spectrum of Fe L x rays.

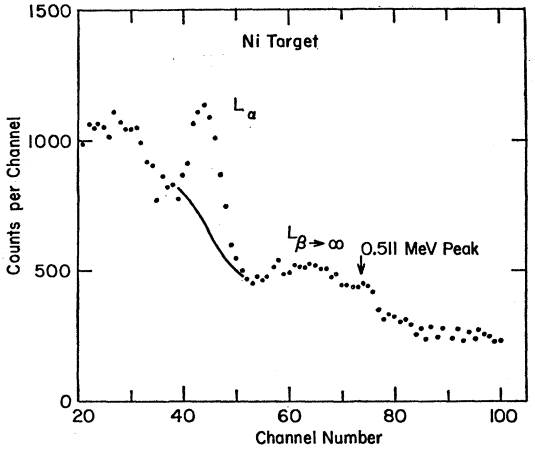

FIG. 14. Pulse-height spectrum of Ni L x rays.

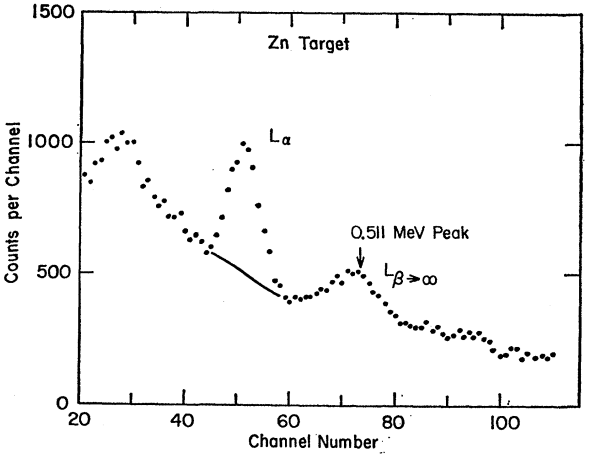

FIG. 15. Pulse-height spectrum of Zn L x rays.

V. DATA ANALYSIS

The procedure followed in analyzing the spectra for the K_α photopeak positions has been described in detail in reference 1. In the present experiment, the data reduction time was greatly reduced by using an IBM-1620 computer. In addition to calculating the mean peak positions, the second and third moments of the photo-

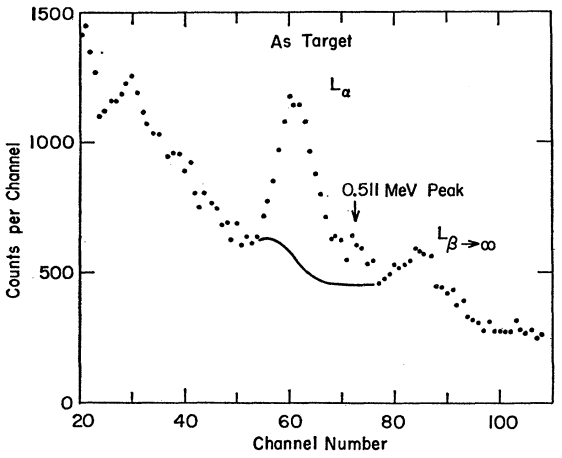

FIG. 16. Pulse-height spectrum of As L x rays.

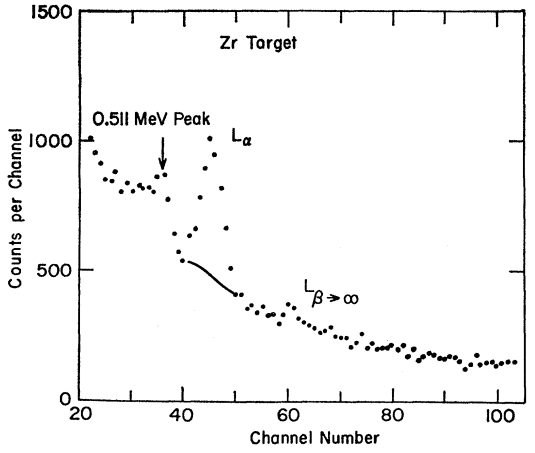

FIG. 17. Pulse-height spectrum of Zr L x rays.

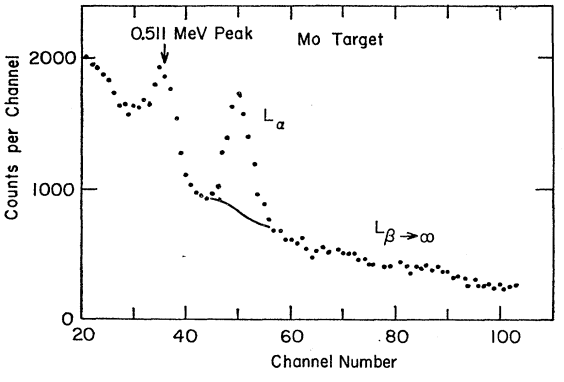

FIG. 18. Pulse-height spectrum of Mo L x rays.

peaks after subtractions were also calculated. The second moment yields the counter resolution and any possible broadening due to fine structure and nuclear quadrupole effects. The third moment gives information about the symmetry of the photopeaks. For the calibration runs the third moments of the peaks were

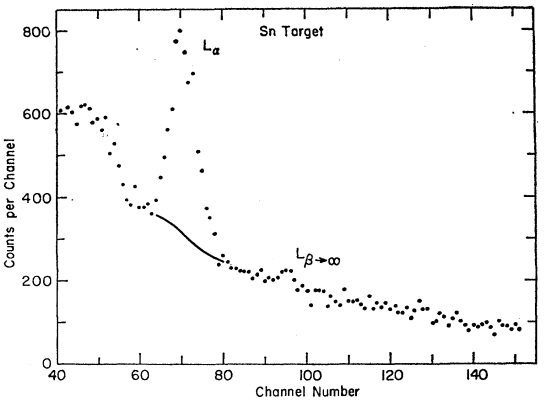

FIG. 19. Pulse-height spectrum of Sn L x rays.

required to be small, within the limits of statistical uncertainty. For the data runs the statistical uncertainties were too large to attach much meaning to the value of the third moment. For the elements Mg through Ca, a spectrum taken using carbon as a target was used for random background subtraction. The background for the remaining elements was taken from above the K peaks, assuming a $1/E$ rule as in reference 1.

The subtraction for the L photopeaks cannot be calculated as reliably as for the K peaks and we had to use a more approximate procedure. We calculated the contribution from the external Compton effects as before but used a straight line extrapolation for the continuous background under the peak. The slope of the straight line was adjusted so that the distribution under the photopeak joined the continuous spectrum above and below the peak. The mean peak position was then calculated in the usual way after this subtraction.

Tables II and III list, for each run, the mean channel positions of the various gamma-ray sources used in calibrating the spectrometer. The results of the Na^{22} calibration runs are given in Table II, and the data from the Hg^{203}, Cs^{137}, ThC″, and PoBe gamma sources are in Table III. The first column of Table II gives the run number, and columns two and three give the mean channels and their statistical uncertainties for the 0.5110- and 1.2736-MeV gammas, respectively. In Table III, the run number is given in the first column, the pulse-height analyzer gain in the second, and the last column gives the mean channel position and its uncertainty for the given source. Two numbers are given to identify the pulse-height analyzer gain. The first gives the conversion gain in volts per 100 channels, and the second gives the amplifier gain as a fraction of full gain. The statistical uncertainties for the calibration and target data runs were calculated as described in reference 1.

Since the counting rates were different for the calibration data and target data runs it was necessary to determine how this might affect the calibrations. Tests

TABLE II. Na^{22} calibration data.

Run No.	0.510976[a] MeV Peak	1.2736[b] MeV Peak
	P.H.A. gain = (1,1)	
104	140.36 ±0.04	353.70 ±0.08
106	140.44 ±0.04	353.96 ±0.09
109	140.06 ±0.04	353.35 ±0.08
111	141.01 ±0.04	353.97 ±0.08
113	139.65 ±0.04	352.78 ±0.08
115	139.71 ±0.04	352.75 ±0.08
117	139.57 ±0.04	352.26 ±0.08
140	139.47 ±0.04	352.00 ±0.08
142	138.92 ±0.04	352.53 ±0.08
146	139.07 ±0.04	351.40 ±0.08
148	139.14 ±0.04	351.23 ±0.08
152	139.13 ±0.04	351.27 ±0.08
154	139.14 ±0.04	351.55 ±0.09
156	139.02 ±0.04	351.32 ±0.09
158	138.93 ±0.04	350.98 ±0.09
186	138.47 ±0.04	350.02 ±0.08
188	138.29 ±0.04	349.80 ±0.08
190	138.29 ±0.04	349.74 ±0.08
192	138.22 ±0.04	349.53 ±0.08
194	138.15 ±0.04	349.32 ±0.08
196	138.25 ±0.04	349.42 ±0.08
198	138.26 ±0.04	349.49 ±0.09
200	138.07 ±0.04	349.29 ±0.09
202	138.13 ±0.04	349.10 ±0.08
204	138.12 ±0.04	349.18 ±0.09
206	138.06 ±0.04	349.33 ±0.09
208	138.12 ±0.04	349.09 ±0.08
239	137.73 ±0.04	348.63 ±0.07
243	137.87 ±0.04	348.81 ±0.07
263	137.12 ±0.04	347.24 ±0.08
265	136.93 ±0.04	346.97 ±0.09
Mean width	σ = 24.1 ±1.1 keV	42.0 ±1.1 keV
	P.H.A. gain = (2.1)	
93	73.31 ±0.02	181.40 ±0.03
95	73.38 ±0.03	181.67 ±0.06
97	73.25 ±0.02	181.32 ±0.04
99	73.11 ±0.02	180.95 ±0.04
103	72.91 ±0.02	180.59 ±0.04
134	72.64 ±0.02	179.74 ±0.04
137	72.58 ±0.02	179.97 ±0.04
149	72.36 ±0.02	179.45 ±0.04
151	72.39 ±0.02	179.37 ±0.04
183	72.00 ±0.02	179.77 ±0.04
185	72.00 ±0.02	178.81 ±0.05
247	71.25 ±0.02	178.27 ±0.05
249	71.81 ±0.02	178.45 ±0.04
Mean width	σ = 24.2 ±2.0 keV	42.8 ±2.0 keV
	P.H.A. gain = (2,1/2)	
160	35.84 ±0.01	91.23 ±0.02
175	35.82 ±0.01	91.23 ±0.02
211	35.53 ±0.01	90.50 ±0.02
218	35.45 ±0.01	90.40 ±0.02
222	35.41 ±0.01	90.38 ±0.02
254	35.49 ±0.01	90.45 ±0.02
262	35.45 ±0.01	90.48 ±0.02
Mean width	σ = 25.4 ±4.0 keV	42.6 ±4.0 keV

[a] W. H. Barkas and A. H. Rosenfeld, University of California Radiation Laboratory Report UCRL-8030, 1958 (unpublished).
[b] P. P. Singh, H. W. Dosso, and G. M. Griffiths, Can. J. Phys. **37**, 1055 (1959).

TABLE III. Calibration data.

Run No.	P.H.A. gain	Mean peak channel
	Hg^{203} (0.27912 ±0.00005 MeV)[a]	
240	(1,1)	72.19 ±0.11
242	(1,1)	72.00 ±0.17
	Mean width σ = 17.2 ±1.1 keV	
	Cs^{137} (0.66160 ±0.00014 MeV)[b]	
244	(1,1)	180.14 ±0.03
	Mean width σ = 29.1 ±1.0 keV	
	ThC″(ThO_2) (2.61425 ±0.00050 MeV)[c]	
159	(2,1/2)	186.16 ±0.07
162	(2,1/2)	186.30 ±0.07
164	(2,1/2)	186.29 ±0.07
166	(2,1/2)	186.29 ±0.07
168	(2,1/2)	186.36 ±0.08
170	(2,1/2)	186.25 ±0.07
172	(2,1/2)	186.16 ±0.07
174	(2,1/2)	186.44 ±0.12
212	(2,1/2)	184.69 ±0.07
220	(2,1/2)	184.51 ±0.10
256	(2,1/2)	184.78 ±0.08
258	(2,1/2)	184.92 ±0.07
260	(2,1/2)	184.63 ±0.10
	Mean width σ = 64.2 ±4.0 keV	
	C^{12*}(PoBe source) (4.425 ±0.020 MeV)[d]	
213	(2,1/2)	306.60 ±0.20
217	(2,1/2)	307.76 ±0.10
221	(2,1/2)	307.40 ±0.08
261	(2,1/2)	308.11 ±0.06
	Mean width σ = 82.0 ±4.0 keV	

[a] K. Edvarson, K. Siegbahn, and A. H. Wapstra (unpublished). G. J. Nijgh, A. H. Wapstra, L. Th. M. Ornstein, N. Salomons-Grobben, J. R. Huizenga, and O. Almen, Nucl. Phys. **9**, 528 (1958–1959).
[b] D. E. Muller, H. C. Hoyt, D. J. Klein, and J. W. M. DuMond, Phys. Rev. **88**, 775 (1952).
[c] G. Lindstrom, Phys. Rev. **87**, 678 (1952).
[d] W. R. Mills, Jr., and R. J. Mackin, Jr., Phys. Rev. **95**, 1206 (1954).

made on the spectrometer system showed that there was a base line shift which shifted the gamma photopeaks to higher channels with increased rate of energy deposition in the NaI crystal. A special study was made using a Na^{22} source at varying distances from the NaI crystal, from which the following relationship between the rate of energy deposition (J) and base line shift (ϵ) was obtained:

$$\epsilon = (13.2 \pm 1.1) \exp[-(42.5 \pm 3.7)/J^{1/2}] \text{ keV}, \quad (2)$$

where J is in MeV/sec.

Table IV gives a summary of the rate effect corrections estimated, using Eq. (2) and the measured J. The first column gives the name of the source, the second gives J, and the third gives ϵ together with its uncertainty. The last two rows of Table IV give the information obtained from target runs at full-beam intensity and 61% of full intensity. There was essentially no difference in J for the various targets used. In making corrections, all runs were converted to the Na^{22} J.

While this procedure serves in the case of the calibration runs where the rate of energy deposition is steady, it does not take proper account of the nonuniform rate of energy deposition during the target runs. This effect was made small by the use of a vibrating target and an electronic gate synchronized to it so as to accept only the more uniform part of the beam pulse. However, an internal check of the calibration which is afforded by the[11] L_α x-ray data, which was taken simultaneously with the K_α x-ray data, to be described, showed that the effect was small.

The precise determination of the energies was plagued by shifts in the calibration peaks during the

TABLE IV. Rate effect correction data.

Source	J (MeV/sec)	ϵ (keV)
Hg^{203}	72.0	0.088±0.038
Co^{137}	4.05×10^3	6.76 ±0.69
Na^{22}	1.58 ± 10^3	4.53 ±0.57
Th^{232}	8.03×10^2	2.94 ±0.46
PoBe	3.42×10^2	1.32 ±0.29
Target[a]	6.08×10^2	2.36 ±0.40
Target[b]	3.69×10^2	1.45 ±0.30

[a] Target run with full-beam intensity.
[b] Target run with 61% full-beam intensity.

[11] L_α as used here refers to the transitions $3d_{5/2}-2p_{3/2}$, $3d_{3/2}-2p_{3/2}$, and $3d_{3/2}-2p_{1/2}$. In x-ray notation these are referred to as $L_{\alpha1}$, $L_{\alpha2}$, and $L_{\beta1}$, respectively, but for simplicity we refer to the sum of these three lines as L_α, i.e., $L_\alpha = L_{\alpha1}+L_{\alpha2}+L_{\beta1}$.

course of the experiment. Calibration points were always measured before and after each target run. In some instances the shift in the peak positions before and after was appreciable. Data were rejected for runs during which the 1.27-MeV peak of Na^{22} had shifted by 3 keV or more. In all, 7 out of 47 runs had to be excluded for this reason. The energies were determined from the mean of the peak position obtained before and after target run of the two lines of Na^{22} (0.5110 MeV and 1.2736 MeV) assuming a linear dependence of energy with channel number. Deviations from nonlinearity in the response of the spectrometer were taken into account by observing the lines of Hg^{203}(0.2791 MeV) (runs 240 and 242 of Table III) and of Cs^{137}(0.6616 MeV) (run 244 of Table III) as well as the Na^{22} lines (runs 239 and 243 of Table II). A three parameter least-squares analysis of these data gives

$$E'=15.784+3.5839C+6.630\times10^{-5}C^2 \text{ keV}, \quad (3)$$

where C is the channel position. The mean-squared error is given by

$$(\Delta E')^2=5.0685-0.10614C+8.0435\times10^{-5}C^2 -2.6319\times10^{-6}C^3+3.3178\times10^{-9}C^4. \quad (4)$$

A two-parameter fit to the Na^{22} data alone gives

$$E''=12.73+3.616C \text{ keV}, \quad (5)$$

and

$$(\Delta E'')^2=1.517-2.136\times10^{-2}C+0.766\times10^{-4}C^2. \quad (6)$$

The difference between the estimates of energy given by Eqs. (3) and (5) represents the correction for nonlinearity:

$$\Delta E=3.17-8.92\times10^{-3}E+5.07\times10^{-6}E^2 \text{ keV}, \quad (7)$$

where the conversion from channels to energy was made using Eq. (5). For the error we simply used the sum of Eqs. (4) and (6) even though these relations are not independent.

As the gamma energy was increased, the spectrometer

TABLE V. Energies of K_α μ-mesonic x rays.

Element	Run No.	Calibrations used	Mean channel C	Correction[a]	$(\Delta E^2)^{1/2}$	Energy (keV)
Mg	189	188, 190	78.36±0.11	1.0±0.9	1.25	295.9±1.6
	199	198, 200	77.96±0.11		1.25	294.6±1.6
	264	263, 265	77.55±0.11		1.24	296.1±1.6
Al	105	104, 106	93.99±0.17	0.7±0.7	1.15	345.9±1.5
	108	106, 109	93.96±0.17		1.12	346.2±1.5
	102	99, 103	49.39±0.12	0.7±0.7	1.25	344.5±2.4
Si	197	196, 198	107.68±0.19	0.4±0.5	0.98	401.0±1.4
	205	204, 206	107.21±0.18		0.98	399.9±1.4
P	193	192, 194	123.47±0.20	0.1±0.3	0.89	457.9±1.3
	203	202, 204	123.70±0.19		0.87	459.0±1.3
S	187	186, 188	140.64±0.16	−0.1±0.2	0.73	522.4±1.2
	195	194, 196	140.44±0.16		0.74	521.5±1.2
Cl	191[b]	190, 192	158.81±0.45	−0.3±0.3	1.71	584.9±2.0
	201	200, 202	158.02±0.21		0.90	582.6±1.3
	207	206, 208	158.00±0.22		0.94	582.6±1.4
Ca	141	140, 142	217.21±0.26	−0.7±0.9	1.50	789.5±1.8
	147	146, 148	217.55±0.26		1.51	792.2±1.8
Fe	114	113, 115	350.15±0.48	0.0±2.5	3.57	1264.2±3.7
	116	115, 117	349.67±0.47		3.55	1263.5±3.7
	153	152, 154	348.25±0.44		3.49	1262.3±3.6
	155	154, 156	347.24±0.41		3.44	1258.5±3.6
	157	156, 158	347.38±0.43		3.48	1260.0±3.6
	136	134, 137	178.36±0.21	0.0±2.5	3.46	1262.3±4.0
	184	183, 185	177.35±0.23		3.52	1263.3±4.0
Ni	96	95, 97	205.22±0.35	0.9±3.6	4.92	1441.6±5.3
Zn	94	93, 95	229.46±0.45	2.0±4.7	6.25	1613.4±6.6
	98	97, 99	229.28±0.42		6.16	1615.7±6.5
As	150	149, 151	263.39±0.45	4.2±6.9	8.31	1876.2±8.5
	248	247, 249	261.78±0.36		8.08	1873.3±8.3
Zr	163	160, 175, 162, 164	180.54±0.39	···	5.48	2530.4±6.8
	167	160, 175, 166, 168	180.83±0.41		5.40	2534.3±6.7
	169	160, 175, 168, 170	180.75±0.34		4.83	2533.1±6.3
Mo	161	160, 175, 159, 162	193.73±0.28	···	4.09	2718.3±5.7
	165	160, 175, 164, 166	193.81±0.28		3.93	2709.3±5.6
	171[c]	160, 175, 170, 172	193.93±0.43		5.96	2723.1±7.2
	173[c]	160, 175, 172, 174	192.85±0.36		5.07	2706.1±6.5
Sn	214	211, 212, 213	243.53±0.54	···	8.42	3447.5±9.3
	219	218, 222, 220, 217, 221	242.42±0.52		8.16	3456.7±9.1
	255	254, 262, 258, 260, 261	243.68±0.38		6.56	3445.4±7.7
	257	254, 262, 258, 260, 261	243.13±0.38		6.54	3437.5±7.7

[a] Includes nonlinearity only.
[b] Data taken using Kel-F target.
[c] Data taken at 61% beam intensity.

response was found to be increasingly nonlinear. This effect was corrected for in the case of the Zr, Mo, and Sn K_α lines by making three parameter least-squares fits to the data from the higher energy gammas of the ThC'' (2.614 MeV) and PoBe (4.425 MeV) sources as well as Na^{22}.

VI. RESULTS

The results of the analysis of the data of the target runs for the K_α photopeak positions and the corrected energies obtained using the calibration data are shown in Table V. Columns two and three of Table V give the run numbers of the target run and the appropriate calibration runs, respectively. Column four gives the mean channel of the photopeak and its statistical uncertainty, column five gives the total correction for nonlinearity and column six contains the calibration error obtained from the least-squares analysis of the calibration runs cited in column three. Column seven contains the corrected x-ray energies and our estimate of the total error for each run. The statistical error was obtained by adding in quadrature the uncertainty in peak position and the calibration error. The nonlinearity correction error was added in quadrature to these. Errors other than the statistical uncertainties were taken into account by including in quadrature an additional 1.0 keV for the (1,1) gain runs, 2.0 keV for the (2,1) gain runs, and 4.0 keV for the (2,1/2) gain runs. The reproducibility of the data is good. The rms deviation of the individual measurements from their means, for all the data, amounts to 0.2%.

The results obtained from analyzing the L_α photopeaks are given in Table VI, which is exactly analogous to Table V for the K_α results. Due to the greater difficulty in making the correct background subtraction, an uncertainty of 2 keV was added in quadrature to the total statistical error for the (1,1) gain runs, 4 keV for the (2,1) gain runs, and 8 keV for the (2,1/2) gain runs. The measurements of K_α and L_α energies are summarized in Tables VII and VIII. In compiling the final values where more than one run was made at a particular pulse-height analyzer gain, the means of the energies obtained from these runs were calculated weighting the various runs on the basis of their statistical accuracy. This gave a resultant statistical error to which the other errors were added in quadrature.

Our new values show a tendency to be systematically higher than our previous values as well as those reported by others. There are a number of possible systematic errors in this type of measurement. These include gain shifts, shifts in the photomultiplier response, nonlinearities in the photomultiplier or in the analyzer, rate effects, especially those caused by the nonuniform output of the cyclotron, shifts due to Compton scattering in the source and in the detector, and shifts due to background subtraction.

In the present series of measurements we dealt with each of these effects more carefully than previously, as outlined above. An over-all check on the validity of our procedures is obtained from a comparison with theory

TABLE VI. Energies of L_α μ-mesonic x rays.

Element	Run No.	Calibrations	Mean channel	Correction[a]	$(\Delta E^2)^{1/2}$	Energy (keV)
Fe	114	113, 115	71.09±0.31	1.2±1.1	1.74	266.7±2.7
	116	115, 117	70.58±0.30		1.72	264.8±2.6
	153	152, 154	70.14±0.38		1.92	264.3±2.8
	155	154, 156	70.12±0.41		2.01	264.8±2.8
	157	156, 158	69.92±0.31		1.73	264.0±2.6
	136	134, 137	37.64±0.19	1.2±1.1	1.90	263.7±4.4
	184	183, 185	37.13±0.20		1.97	263.2±4.5
Ni	96	95, 97	44.79±0.17	0.9±0.9	1.65	310.8±4.3
Zn	110	109, 111	96.78±0.39	0.6±0.7	1.65	355.0±2.6
	94	93, 95	51.34±0.18	0.6±0.7	1.58	356.5±4.3
	98	97, 99	51.26±0.21		1.71	356.7±4.3
As	150	149, 151	60.62±0.16	0.3±0.4	1.29	427.5±4.2
	248	247, 249	61.16±0.15		1.20	437.3±4.2
Zr	163	160, 175	45.21±0.10	−0.5±0.5	1.55	639.5±8.1
	167	160, 175	45.30±0.11		1.61	640.8±8.2
	169	160, 175	44.98±0.10		1.53	636.4±8.1
Mo	161	160, 175	50.37±0.09	−0.6±0.7	1.56	710.5±8.1
	165	160, 175	50.05±0.09		1.58	706.1±8.1
	171[b]	160, 175	50.17±0.13		2.01	707.7±8.2
	173[b]	160, 175	49.85±0.15		2.24	703.3±8.3
Sn	214	211	70.64±0.13	−0.7±1.6	2.64	997.4±8.4
	219	218, 222	70.47±0.13		2.66	979.2±8.4
	255	254, 262	70.76±0.12		2.62	999.6±8.4
	257	254, 262	70.88±0.13		2.64	1001.3±8.4

[a] Includes nonlinearity correction only.
[b] Data taken at 61% beam intensity.

TABLE VII. Summary of L_α results.

Element	Mean[a] energy (keV)	Mean width σ (keV)	Theoretical energy (keV)
Fe	265.0±2.4	16.5±2.2	266.6
	263.5±4.2	14.7±4.2	266.6
Ni	310.8±4.3	15.7±4.5	309.6
Zn	355.0±2.6	19.4±2.5	355.7
	356.6±4.2	18.6±4.1	355.7
As	432.7±4.1	25.1±4.1	431.1
Zr	638.8±8.1	25.9±8.1	635.9
Mo	707.5±8.1	34.2±8.0	701.7
Sn	994.6±8.2	41.7±8.1	994.4

[a] Corrected for nonlinearity only.

TABLE VIII. Summary of K_α results.

Element	Mean energy (keV)	Mean width σ (keV)	$R_{eq}/A^{1/3}$ (10^{-13} cm)
Mg	295.6±1.6	17.7±1.2	1.45±0.18
Al	346.1±1.4	22.7±1.2	1.37±0.08
	344.5±2.4	18.1±2.4	1.47±0.09
Si	400.4±1.3	22.0±1.8	1.32±0.09
P	458.5±1.3	23.0±1.2	1.25±0.07
S	522.0±1.2	22.7±1.2	1.16±0.04
Cl	582.8±1.3	25.9±1.2	1.24±0.04
Ca	790.8±1.6	32.9±1.4	1.23±0.03
Fe	1261.4±3.3	42.8±2.2	1.25±0.02
	1262.8±3.9	47.7±2.9	1.24±0.02
Ni	1441.6±6.1	51.0±3.9	1.22±0.02
Zn	1614.6±6.2	47.8±4.4	1.23±0.02
As	1874.4±8.2	50.6±4.6	1.24±0.02
Zr	2534.0±5.1	71.9±5.1	1.23±0.01
Mo	2718.5±4.6	66.3±4.8	1.24±0.01
Sn	3446.4±6.4	79.1±6.5	1.24±0.01

of our measurements of the L_α x rays, which are obtained simultaneously from the same runs which give the K_α x rays. These $3d-2p$ transition energies are given accurately enough by the theory for the elements studied here to serve as a reliable basis of comparison. All the effects which shift the $1s$ level to a somewhat unknown extent, perturb the $2p$ level much less, and the $3d$ level hardly at all. In addition to the experimental values obtained for the $3d-2p$ transition energies we give in Table VII theoretical values calculated as follows: The tabulations of Ford and Wills were used for the $2p_{1/2}$ and $2p_{3/2}$ energies, interpolating where necessary. The $3d_{3/2}$ and $3d_{5/2}$ energies were calculated from the standard formula[12] for the energy levels of a Dirac atom with point nucleus,

$$E_{n,j}=-\frac{1}{2}\frac{\bar{\mu}c^2}{n^2}\alpha^2Z^2\left[1+\frac{(\alpha Z)^2}{n}\left(\frac{1}{j+\frac{1}{2}}-\frac{3}{4n}\right)+\cdots\right], \quad (8)$$

where $\bar{\mu}$ is the reduced mass of the meson. Corrections for vacuum polarization were made from the work of Pustovalov[13] and of Koslov.[14] The correction for the effect of the finite nuclear size was negligible. The $3d-2p$ transition energies were calculated by taking the difference of weighted averages:

$$E(3d)=\tfrac{3}{5}E(d_{5/2})+\tfrac{2}{5}E(d_{3/2}), \quad (9)$$

$$E(2p)=\tfrac{2}{3}E(p_{3/2})+\tfrac{1}{3}E(p_{1/2}). \quad (10)$$

In the case of Sn ($Z=50$), for example, the nonrelativistic energy of the $3d$ level is -780.7 keV. Relativity and spin effects lower this by 5.3 keV, while the effect of the vacuum polarization decreases it further by 2.6 keV. The corrections are correspondingly smaller for the other elements on our list, all of which have lower Z.

The presence of a $3p-2s$ transition could perturb the L energy measurement.[15] In Fe the energy difference $(3d-2p)-(3p-2s)$ is 23.5 keV, within the experimental spread of the L_α line. We have been able to estimate that the $3p-2s$ transition contributes only about 4% to the total intensity of the observed line. This would lower the observed L_α energy by about 1 keV. The effect lies within the uncertainty of the background subtraction and we have not explicitly applied this correction to the values listed in Table VII. For higher Z the overlap of the satellite line becomes less, reducing the effect on the position of the main line. For Sn the energy difference is 258 keV, large enough to be well outside the wings of the L_α line for this element.

The agreement between the experimental and the theoretical values is within the experimental error in every case. Due to the larger experimental error associated with these measurements, the test is not as critical as one would like to have it. However, taking all the measurements as a group, the experimental values were found, on the average, to be 0.5 ± 1.3 keV lower than those calculated from theory. This good agreement lends confidence to general procedure of energy measurement used here. It indicates that systematic shifts such as might be caused by a rate effect from the nonuniform output of the cyclotron are probably within the limits of error given.

The results of the present series of measurements of the $2p-1s$ transition energies are also presented in Table IX. For comparison, our previous measurements are listed in addition, as well as those reported by others. The agreement with our previous results is good, with two exceptions. In the case of Zn, the new value is 1.7% higher than that given in reference 1, while the new value for Ni is 1.5% higher than the old. In both cases the discrepancy has an uncomfortably low expectation in view of the stated errors. We suspect a nonlinearity in the spectrometer response at energies above the highest calibration point (1.33 MeV) of the previous experiment as a possible cause for these discrepancies.

For comparison with the experimental results we have listed in column 8 of Table IX the calculated values given by Ford and Wills, or values interpolated from their tabulations. As in reference 1 we show in Fig. 20 the deviation of the measured values from those obtained from Ford and Wills. Here the new values are plotted together with those of the older values which were not remeasured in the new series. It is seen that the discrepancy which we reported in reference 1 is confirmed here. It rises from a small value at Mg ($Z=12$) to a maximum of almost 3% at Ca ($Z=20$) and then falls off slowly with increasing Z.

We have already remarked that the principal fault of the Ford and Wills calculation was their particular choice of charge distribution. Better agreement with our data is obtained using either of the shapes chosen by Hofstadter and his collaborators,[5] with parameters chosen to fit the Stanford scattering data. The pertinent calculations of the energy levels have been made by Pustovalov and Krechko.[16] In Table IX we list, by way of comparison with our measurements, their values calculated for the so-called Fermi type of charge distribution having the form,

$$\rho(r)=\frac{\rho_0}{1+\exp[(r-c)/z]} \quad (11)$$

with values of the parameters,

$$c=1.08A^{1/3}\times10^{-13}\text{ cm}$$

[12] See, for example, L. I. Schiff, *Quantum Mechanics* (McGraw-Hill Book Company, Inc., New York, 1955), 2nd ed., p. 337.

[13] G. E. Pustovalov, Zh. Eksperim. i Teor. Fiz. **32**, 1519 (1957) [translation: Soviet Phys.—JETP **5**, 1234 (1957)].

[14] S. Koslov, NEVIS Cyclotron Laboratory Report, NEVIS-19, 1956 (unpublished).

[15] We are indebted to Professor Gregor Wentzel for drawing our attention to this point.

[16] G. E. Pustovalov and M. S. Krechko, Nucl. Phys. **19**, 337 (1960).

TABLE IX. Summary of measured and calculated μ-mesonic $2p-1s$ transition energies.

		Measured					Calculated		
Element	Z	This experiment	Chicago[a]	CERN[b]	Columbia[c]	Columbia[d]	Los Alamos[e]	Moscow[f]	Ottawa[g]
Mg	12	295.6±1.6					294.4	296	296.1
Al[h]	13	345.7±1.2	344.2±9.1			350	344.3	346	
Si	14	400.4±1.3					397.0	399	398.8
P	15	458.5±1.3					452.4	455	
S	16	522.0±1.2		516±4			512.0	515	515.2
Cl	17	582.8±1.3					572.0	578	
K	19		721.5±5.7	714±3			702.7	711	
Ca	20	790.8±1.6	788.9±5.3	784±3			771.8	782	782.2
Ti	22		935.9±2.6	937±7	924.7±2.5	955	920.2	931	
Cr	24		1094.4±4.3				1074.5	1087	
Mn	25		1178.1±4.3	1174			1156.3	1169	
Fe[h]	26	1262.0±2.5	1257.6±4.3	1258±6	1255.5±2.4		1239.1	1253	
Co	27		1332.8±4.3	1337±5			1323.0	1339	1342.5
Ni	28	1441.6±6.1	1421.9±5.0	1426			1411.3	1424	1417.7
Cu	29		1511.0±5.5	1515	1508.2±4.0	1550	1498.1	1509	
Zn	30	1614.6±6.2	1586.7±4.4	1600	1586.9±4.5		1588.3	1598	
As	33	1874.4±8.2		1867±7			1853.0	1872	
Zr	40	2534.0±5.1					2516.6	2533	
Mo	42	2718.5±4.6		2712±5			2715	2718	
Rh	45			2977					
Pd	46			3068					
Ag	47			3163			3201		
Cd	48			3254			3293		
In	49			3360			3366		3392
Sn	50	3446.4±6.4		3454			3466	3470	
Sb	51			3546		3500	3543		3553.3
Ba	56			3985±30			3996		
La	57			4079			4084		

[a] Reference 1.
[b] P. Brix, R. Engfer, U. Hegel, D. Quitmann, G. Backenstoss, K. Goebel, and B. Stadler, Phys. Letters 1, 56 (1962).
[c] W. Frati and J. Rainwater, Phys. Rev. 128, 2360 (1962).
[d] V. L. Fitch and J. Rainwater, Phys. Rev. 92, 789 (1953).
[e] Reference 2. The numbers given here are from the second reference and differ in several cases from those given in the first reference.
[f] From curve for Fermi model with average parameters Fig. 1, Reference 16.
[g] F. J. Bloore, Y. P. Varshni, and J. M. Pearson (to be published).
[h] Weighted mean of the two energies (Table VIII) assuming the two values to be independent.

and

$$z=0.545\times10^{-13}\text{ cm},$$

which are a reasonable average of the values found by Hofstadter *et al.*[5,7] for the elements they studied with $A>16$. Bloore, Varshni, and Pearson (reference g, Table IX) have estimated for several elements the perturbation to the $2p-1s$ transition energy produced by the replacement of the Ford and Wills distribution by that chosen by the Stanford group. The approximate wave functions given by Pustovalov[17] were used. When these energy shifts are added to the Ford and Wills values the values given in the last column of Table IX are obtained. It can be seen that the discrepancy between measurement and calculation is considerably reduced when the Stanford charge distributions are used. A difference still remains near K and Ca but this is now only 1.2%, smaller than it was by a factor of 2. Because of the uncertainty in the shape of the nuclear charge distribution it remains an open question whether our results are outside the range allowed by charge distributions which are consistent with the electron scattering results. In view ot this, we considered it to be more meaningful to determine the values of the nuclear radii which are consistent with our measurements.

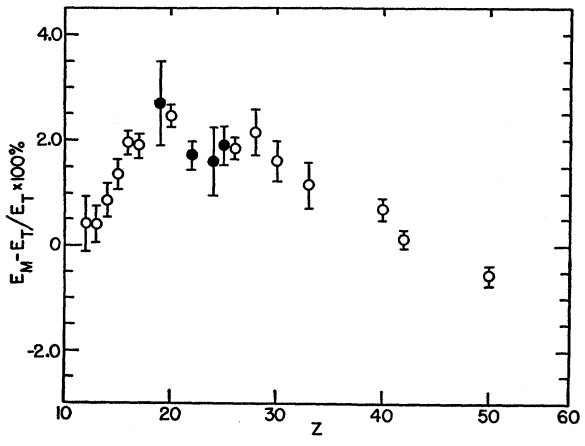

FIG. 20. Plot of the percent deviation of the measured K energies (E_M) from the theoretical values (E_T) computed by Ford and Wills (reference 2). The open circles are from the present experiment and the full circles are from the previous experiment (reference 1). Data for Co($Z=27$) and Cu($Z=29$) were obtained in the previous experiment but are not shown in this plot since they are believed to be unreliable. The indicated errors represent the total estimated uncertainties.

[17] G. E. Pustovalov, Zh. Eksperim. i Teor. Fiz. **36**, 1806 (1959) [translation: Soviet Phys.—JETP **36**, 1288 (1959)].

The shift in the $2p-1s$ transition energy is a measure, primarily, of the mean-square radius of the nuclear-charge distribution.[4,18] More precisely, Pustovalov[17] has given a formula from which the shift in energy, due to the finite extension of the charge, can be calculated fairly reliably even when the nuclear charge extends quite far into the region occupied by the mesonic orbits.

The Pustovalov formula gives the quantum defect as a function of the parameter $t=(\bar{\mu}e^2ZR_{eq})/\hbar^2$. For the $1s$ state it is

$$\Delta n(1s)=-0.032885+0.165892t+0.013883t^2 -0.008312t^3+0.001082t^4+0.032885 \times\exp(-5.0446t-0.9826t^2+0.5560t^3 -2.9875t^4). \quad (12)$$

For the $2p$ state it is

$$\Delta n(2p)=-0.0033673t^2+0.0087840t^3-0.0019263t^4 +0.0001244t^5+0.0033673t^2 \times\exp(-2.6086t-0.7091t^2-0.7000t^3). \quad (13)$$

The energy is obtained from

$$E=E_0(n+\Delta n)^{-2}, \quad (14)$$

where $E_0=-\bar{\mu}e^4Z^2/2\hbar^2$ is the nonrelativistic energy of the ground-mesonic atom state for the point nucleus.

In Fig. 21 we give the dependence of $(-\Delta E/E)/(\Delta R_{eq}/R_{eq})$ as a function of Z from this formula. These deviations are calculated for values of $E(2p-1s)$ and $R_{eq}=[(5/3)\langle r^2\rangle]^{1/2}$ near those given by Ford and Wills. Values of $(-\Delta E/E)/(\Delta R_{eq}/R_{eq})$ obtained by direct calculation by Ford and Wills are in good agreement with the curve of Fig. 21.

Using Ford and Wills' calculations as a base, we determined the change in R_{eq} required to bring the Ford and Wills energy values into agreement with our measurements. In this way, we were able to arrive at values of nuclear radii which are consistent with our K_α energies, provided that other nuclear effects are unimportant. In column four of Table VIII the values of $R_{eq}/A^{1/3}$ derived in this way are listed.[18a] Here $R_{eq}=(5\langle r^2\rangle/3)^{1/2}$ is the radius of an equivalent uniform spherical charge distribution having the same value of $\langle r^2\rangle$. It is seen that the values of $R_{eq}/A^{1/3}$ are remarkably constant down to $A=32$ (S). A comparison of our values and those obtained by Hofstadter[7] from the electron scattering experiments, is shown in Fig. 22. There is no clear disagreement between the two sets of values and Hofstadter's general conclusion that the nuclear-charge density stays essentially constant above $A=12$ is unaltered by our results.

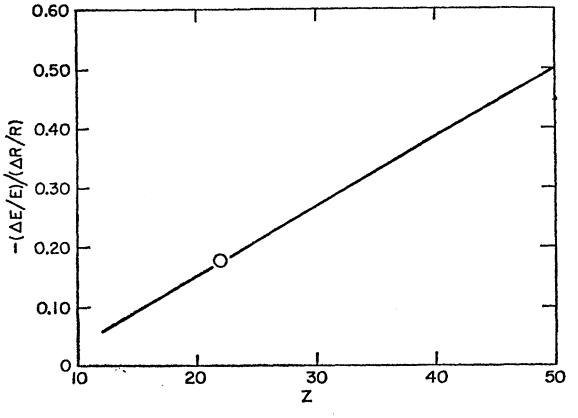

FIG. 21. Plot of the fractional change in K_α energy divided by the fractional change in nuclear radius against Z. The dependence is linear over our range of interest ($Z=12$ to 50). The circled point is the value for Ti($Z=22$) calculated by Ford and Wills.

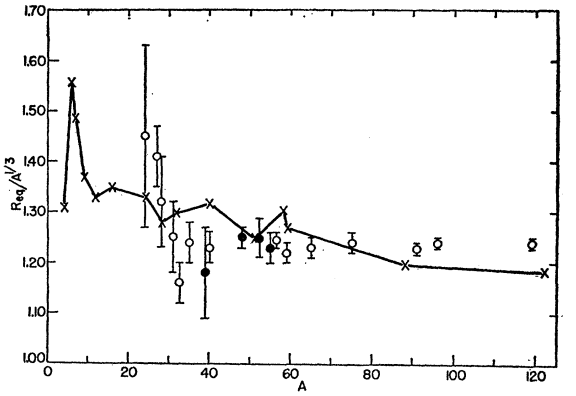

FIG. 22. Plot of $R_{eq}/A^{1/3}$ vs A for values obtained from this experiment (open circles) and our previous experiment (reference 1) (full circles). Also plotted are the equivalent radii obtained from electron scattering experiment (references 5 and 7) (crosses). The electron scattering values are shown connected by straight lines to make them easier to follow on the figure.

VII. PERTURBING EFFECTS

A. Linewidth

In this experiment we tried to see whether the splitting due to fine structure or quadrupole interaction effects[19–21] could produce a noticeable broadening in the linewidth. We calculated, for each of the calibration gamma ray lines, the standard (rms) deviation of the measured points of the line. That is, we calcuated the width

$$\sigma=[\textstyle\sum_i(E_0-E_i)^2N_i/\sum_i N_i]^{1/2}, \quad (15)$$

where E_0 is the mean energy of the line, and E_i is the energy corresponding to the ith channel in which there

[18] D. L. Hill and K. W. Ford, Phys. Rev. **94**, 1617 (1954). These authors showed that if relativistic effects are taken into account exactly, it is $\langle r^{2s}\rangle$ that is determined with $s=(1-\alpha^2Z^2)^{1/2}$.

[18a] *Note added in proof.* R. McKee has confirmed these values for the equivalent radii by direct numerical solution of the Dirac equation using an IBM 7090 computer.

[19] L. Wilets, Kgl. Danske Videnskab. Selskab, Mat.-Fys. Medd. **29**, No. 3 (1954).

[20] B. A. Jacobsohn, Phys. Rev. **96**, 1637 (1954).

[21] J. A. Wheeler, Phys. Rev. **92**, 812 (1953).

were N_i net counts. The relation between σ and the energy of the line

$$\sigma = 36.2E^{0.569}\ \text{keV}, \quad (16)$$

with E in MeV, fits all the calibration lines within their uncertainties, and so is valid over the range from 0.3 to 4 MeV.

The standard deviations were also calculated for the observed x-ray lines. The mean value of σ is tabulated for each of the elements measured in this experiment in Table VIII for the K_α lines and in Table VII for the L_α lines. The K_α linewidths are plotted in Fig. 23 together with the widths obtained from the calibration gamma-ray lines and the fit [Eq. (16)] to the latter. Two points are plotted in the case of Al and Fe, one for each of two gain settings which were used in these cases. We find no clear evidence for a broadening of any of the K_α lines. The widths of the L_α lines also are consistent with Eq. (16) although the uncertainties in width are larger.

To obtain some idea of the magnitude of the effect of the splitting of the lines we calculated the broadening to be expected for the case of $_{49}In^{115}$, a nucleus with a relatively high quadrupole moment among those known in this region of the table of elements. In this case, the splitting would appear as a broadening of the inherent width by 4% mainly due to the fine structure, but this would be undetectable since the uncertainty in our measurement of the width is larger, about 8% in this region of Z. The splitting is relatively more important for the L_α lines, but here, because of the poorer accuracy in determining the line, the presence of the effect was concealed also. The situation is quite different for the heavier elements where we have been able to report a quite clear broadening effect.[22] A considerable improvement in resolving power would be required to reveal the quadrupole effects clearly.

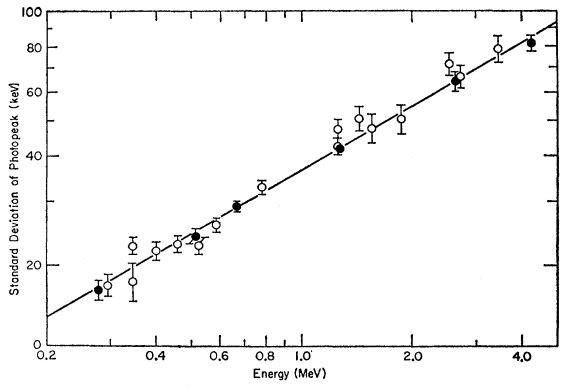

FIG. 23. Log-Log plot of the mean standard deviations (σ) vs energy (E) of the photopeaks from the calibration runs (full circles) and K_α energy runs (open circles). Also shown is the curve obtained from a least-squares fit to the calibration points [Eq. (16)].

[22] E. P. Hincks, Bull. Am. Phys. Soc. **5**, 427 (1960).

B. Nuclear Deformation

Splitting of the $2p$ level would not affect the energy determinations in the experiment, the analysis giving in each case the centroid of the line. There is, however, a shift in energy which would be brought about by the distortion in the nuclear shape which is revealed by, and must be present, if the nucleus has a quadrupole moment. The energy shift depends primarily on the amount that $\langle r^2 \rangle$ would change in the distorted nucleus.

It would therefore show up as a discrepancy between an observed transition energy and a theoretical value based on the value of $\langle r^2 \rangle$ or R_{eq} appropriate to a spherical nucleus of the same A. Conversely, a distortion would be observed as a shift in the value of R_{eq}, whether determined from a μ-mesonic transition or from electron scattering and we may look for fluctuations in the value of $R_{eq}/A^{1/3}$ for evidence of it. We do not, of course, expect to see any discrepancy between a measured transition energy and one calculated from an experimental value of $\langle r^2 \rangle$, as are those given in Table IX. The magnitude of the deformation effect depends on the nuclear model used to account for the origin of the quadrupole moment. According to the present picture,[23,24] the closed-shell nuclei have zero-quadrupole moments, while in the vicinity of the closed shells the quadrupole moment is small and can be accounted for by the distribution of the extra protons, with zero or small deformation of the nuclear core. Far from the closed shells, quite substantial deformations of the core are required to account for the large quadrupole moments which are observed. It is, in these cases, that a calculation of the energy levels based on a spherical model might need modification.

Nuclei with spin 0 or 1/2 in their ground state which do not have an observed quadrupole moment may also be nonspherical. Their deformation which, through the collective motion of nucleons can give rise to rotational states, may be deduced from the energies of these states or from the electric quadrupole transition rates between them. It would appear that the intrinsic deformations of these nuclei in their ground state are of approximately the same magnitude as those revealed by the static quadrupole moments of neighboring nuclei having a spin $>1/2$.

We estimated the magnitude of the possible energy shift by supposing that all the quadrupole moment was due to a deformation of a homogeneous and incompressible charge distribution in the form of an ellipsoid of revolution cylindrically symmetric about the axis defined by the total angular momentum. We found that the energy shift produced was quite small,

[23] M. Goeppert-Mayer, in *Proceedings of the International Conference on Theoretical Physics Kyoto and Tokyo, 1953* (Science Council of Japan, Tokyo, 1954).

[24] A. Bohr, Kgl. Danske Videnskab. Selskab, Mat.-Fys. Medd. **26**, No. 14 (1952); A Bohr and B. R. Mottelson, *ibid.* **27**, No. 16 (1953); and D. L. Hill, in *Handbuch der Physik*, edited by S. Flügge (Springer-Verlag, Berlin, 1957), Vol. 39, p. 178.

within the error of the measurements in all cases for which the quadrupole moment was known. The largest effect occurred for $_{33}As^{75}$ where the energy shift was 4.6 keV. However, in this case, the error assigned to the measurement was 8.3 keV.

C. Nuclear Polarization

Besides the effect of the nuclear distortion, which tends to decrease the binding energy of the nucleus by increasing the value of $\langle r^2\rangle$, there are additional effects which arise because the presence of the meson can alter the state of the nucleus. The nuclear polarization effect, which comes about in this way, tends to increase the binding energy. The polarization energy for a meson in the state k is calculated in second-order perturbation theory by means of the formula[4]

$$W^{(2)}=\sum_{N,m}\frac{\langle\psi_0\phi_k|H'|\psi_N\phi_m\rangle\langle\psi_N\phi_m|H'|\psi_0\phi_k\rangle}{(E_0+\epsilon_k-E_N-\epsilon_m)}, \quad (17)$$

where N and m refer to the entire set of quantum numbers for the nucleus and meson, respectively, with $N=0$ and $m=0$ referring to the ground state. Unfortunately, the calculation of the nuclear polarization is strongly model-dependent and different authors attempting to estimate the effect have obtained widely different results.

The nuclear polarization effect was first estimated rather crudely by Cooper and Henley[4] for the $1s$ state by using closure over both the nuclear and the meson states. To do this they had to take an average value for the energy denominator, and chose the value 13 MeV for (E_0-E_N) from the statistical model. They obtained shifts of -58 keV in Pb, -13 keV in Cu and -1.2 keV in Al. Lakin and Kohn[25] have reported a calculation giving a shift of -16 ± 8 keV for $Z=80$, and point out that correlated motion of the protons can reduce the magnitude of the shift by a large factor. More recently, Nuding[26] carried out a more extensive calculation based on the Steinwedel-Jensen model[27] and found a shift of -8.2 keV for Pb. Moreover, in the case of Pb the shift in the $2p$ level turns out to be -2.7 keV, so that the net effect is to increase the $2p-1s$ transition energy by 5.5 keV. What was a sizeable effect according to Cooper and Henley is reduced by a factor of 10 if Nuding's result is to be believed. For $_{51}Sb$, Nuding gives $\Delta E_{1s}=-4.2$ keV and $\Delta E_{2p}=-0.3$ keV, while the dependence on the nuclear charge is given as $Z^{1.4}$ for the $1s$ state and $Z^{4.6}$ for the $2p$ state. This makes the value for Cu $\Delta E_{1s}=-1.9$ keV, too small to influence our results with their present accuracy. Somewhat larger effects are obtained when nuclear surface oscillations are taken into account. Depending on the choice of surface potential, Nuding calculates $\Delta E_{1s}=-12.8$ or -10.5 keV for Pb and $\Delta E_{1s}=-11.0$ or -8.9 keV for Sb. This would bring the total effect on the $2p-1s$ transition energy near $Z=50$ to be about $+0.5\%$. Our own measurements in this region (i.e., $_{50}Sn$, $_{42}Mo$, and $_{40}Zr$) are already too low compared to what would be calculated from the electron scattering measurements; the polarization correction would only worsen the agreement. More precise measurements will be required before a less ambiguous statement can be made.

[25] W. Lakin and W. Kohn, Phys. Rev. **94**, 787 (1954).
[26] E. Nuding, Z. Naturforsch. **12a**, 187 (1957).
[27] H. Steinwedel and J. H. D. Jensen, Z. Naturforsch. **5a**, 413 (1950).

VIII. CONCLUSION

The measurements of μ-mesonic x-ray energies reported here have been interpreted to give a measure of the extent of the nuclear charge. The $2p-1s$ transition energy depends essentially on the second moment of the charge distribution, somewhat independently of the detail of the shape. From the values of $\langle r^2\rangle$ obtained from our measurements we give values of the radius $R_{eq}=(5\langle r^2\rangle/3)^{1/2}$ of an equivalent sphere of uniform charge distribution in order to compare our results with those obtained from the Stanford electron scattering experiments. Our values of $r_0=R_{eq}/A^{1/3}$ are remarkably constant, within $(1.23\pm0.02)\times10^{-13}$ cm, for all nine of our elements between $A=35$ (Cl) and $A=119$ (Sn). The Stanford values agree with ours in general, but are lower by about 3% at $A=120$, and higher by 7% at Ca ($A=40$). It is not clear to what extent nuclear polarization affects these comparisons. When the nuclear charge distributions obtained from electron scattering on the one hand and from μ-mesonic transitions on the other hand can be compared more accurately it will be interesting to examine the differences in sensitivity to the various perturbing effects. Vogt[28] has recently discussed, for example, evidence that the apparent surface thickness depends on the energy of the probing particle and has interpreted this in terms of a polarization effect. Similarly, we may expect that a high-energy electron and a bound muon will not "see" identical charge distributions.

ACKNOWLEDGMENTS

We wish to thank Professor D. G. Ravenhall, Professor R. Hofstadter, Professor G. Wentzel, and Professor Y. P. Varshni for helpful and enlightening discussions. We would also like to thank Dr. S. Malik, R. Gabriel, and W. Stanula for their help in constructing the apparatus and in conducting the experiment.

[28] E. Vogt, Rev. Mod. Phys. **34**, 723 (1962).